Geological Survey of Japan Cruise Report No. 24, p. 33-50, 1999

IV. HIGH RESOLUTION MULTICHANNEL SEISMIC SURVEY IN THE OFF TOKAI AREA

Shin'ichi Kuramoto, Yukinobu Okamura, Kohsaku Arai and Fumitoshi Murakami

Introduction

High resolution multichannel seismic (here after MCS) surveys were carried out during the GH97 cruise by the R/V Hakurei-maru and the GA97 cruise by the Asia-maru off Tokai, in 1997. The main purpose of the surveys was to get much higher resolution seismic data and to get much deeper crustal images rather than single channel seismic data, that are covering the entire survey area. Fig. IV-1 shows all the

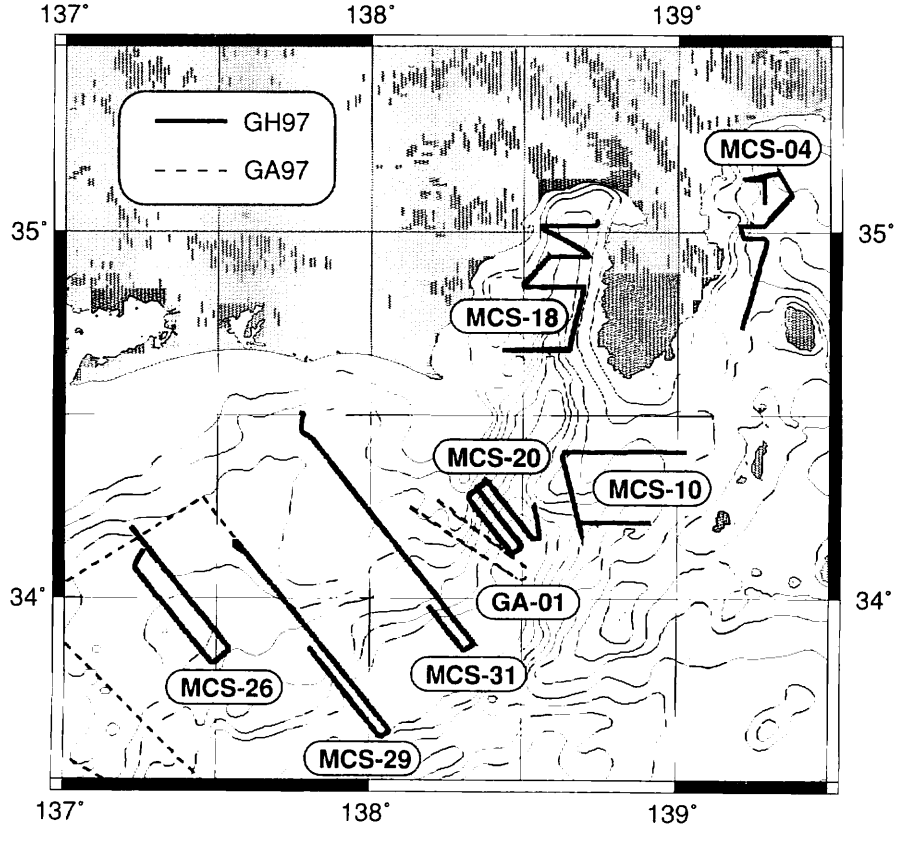

Fig. IV-1 Map with all the MCS track lines of the GH97 and GA97 cruises. Solid lines show the GH97 cruise, and broken lines show the GA97 cruise respectively.

Keywords: Nankai trough, high resolution multichannel seismic survey, active fault, accretionary prism

MCS survey lines of the GH97 and GA97 cruises. MCS data were successfully gathered and processed just after the cruises. This report introduces the preliminary results of MCS data from the off Tokai area.

High Resolution MCS System

What is the high resolution MCS data acquisition system that we are using? Our system is in general focusing on surveys of relatively deep ocean of 1000 m depth or more. We use the following data acquisition system.

1) Sound source >>> Two GI-GUNs (G = 250 cu. in., I = 105 cu. in.; × 2)
2) Streamer Cable >>> 12.5 m spacing, 48-channel solid streamer cable with five depth controllers
3) Recording >>> 24 bits, SEG-D (8048) demultiprexed format
4) Navigation >>> Differential GPS and Glonass complex operation

We were able to detect differential navigation data during the surveys off Tokai. The navigation accuracy is less than 1 m. Manually controlled GI-GUNs are fired every 25 or 50 m. The recording length is 8 seconds, and the sampling interval is 2 msec.

Recorded data are processed as follows.

1) data loading
2) gain recovery
3) band-pass filtering
4) velocity analysis every 300 or 600 m
5) NMO correction
6) stacking
7) band-pass filtering
8) mute
9) f-k migration
10) band-pass filtering
11) auto gain control
12) plotting

This processing procedure is very common as a preliminary processing. Further precise processing, e.g. multiple removal, pre-stack dip move out, finite difference depth migration, etc., are planned as a future work.

We will briefly show the preliminary processed data and point out some interesting features in the basis of selected profiles. Fig. IV-2 illustrates the selected lines that are shown in this report.

West Sagami Bay and the Southern off Izu Peninsula

MCS-04 crosses the Manazuru knoll from the south to the north (Fig. IV-3). The knoll shows a northward dipping antiformal structure that was formed in conjunction with a reverse fault that is seen at its southern foot. Thick sediments exposed in this area are deformed by the reverse fault. It could be an active fault.

MCS-10 runs over the Iro submarine canyon and the Izu spur (Fig. IV-4). The canyon has a NNE-SSW direction, that changes the direction to the west, to the Nankai trough axis, at around 34° 15′ N. The western wall of the Iro submarine canyon (around shot #850) is formed by an active fault scarp. The fault dips to the

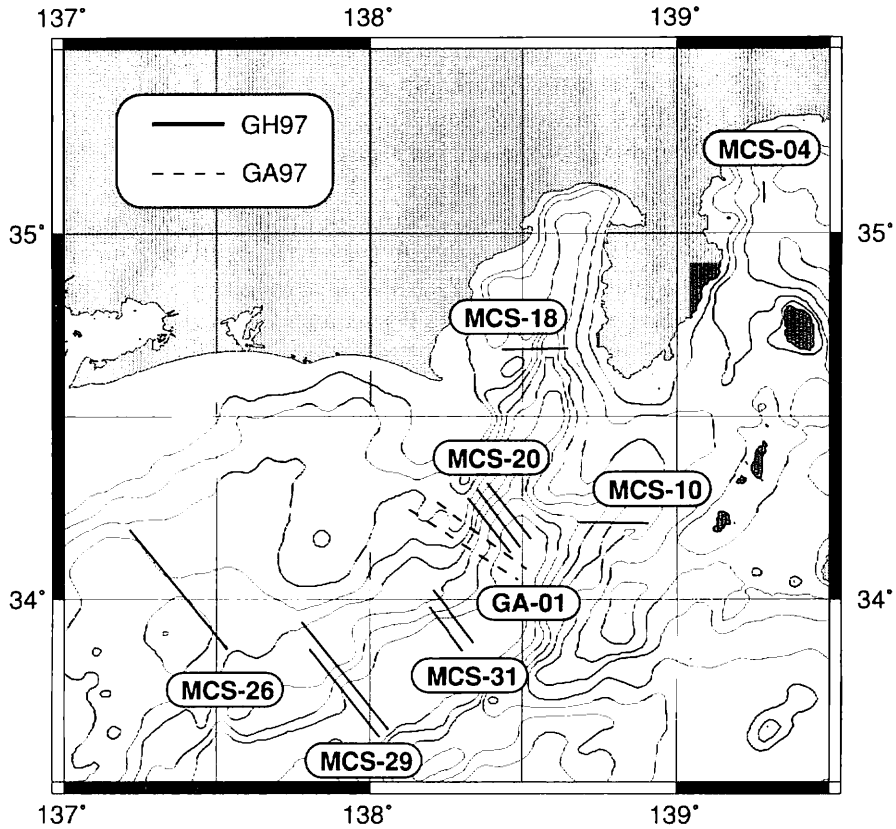

Fig. IV-2 Selected MCS profiles are used in this report. Solid lines show the GH97 cruise, and broken lines show the GA97 cruise respectively.

west and deforms the sediments in the Iro canyon.

Suruga Bay

MCS-18 crosses over the Suruga bay (Fig. IV-5). The eastern block, Izu Peninsula side, tilts to the west and does not show any significant internal structure. The eastern block, however, shows extremely different structures. Some imbricated thrusts and tilted blocks are visible suggesting that the structure resembles that of an accretionary prism. A relatively high amplitude reflector is visible at 0.8 seconds (two-way travel time) depth from seafloor, around shot #350. It is possible to trace it about 5 km to the west. This reflector is interpreted as a décollement reflector, suggesting subduction at the Suruga trough. The western part of profile, at the Senoumi knoll, is characterized by non-deformed sediments of about 0.4 sec. thickness that cover an acoustic basement. The basement shows relatively scattered reflections and looks a chaotic reflector.

Nankai Trough-Suruga Trough Junction

MCS-20 and GA-01 run from the Nankai trough axis to the deformation front of

the accretionary prism. The boundary between the Suruga trough and the Nankai trough occurs here, off the Kanasunose knoll. Fig. IV-6 to IV-10 show the profiles from west to east. The characteristic deformation structures are changing from profile to profile. The trough-fill sediments are about 1 sec. thick and they are deformed at the boundary between the landward slope and the trough (Fig. IV-6, IV-7). There is an unclear thrust, that is, however, not an obvious décollement reflector; the landward block tilts to the northwest. Fig. IV-8 shows a thrust at the boundary, that is no longer visible in fig. IV-9 and IV-10. Striking is the change of deformation structure and the change of subduction vergence from oceanward to landward, shown by the profiles. Fig. IV-8 to 10 do not show typical subduction structures, but rather show obduction structure from ocean side. MacKay *et al.* (1992) reports similar structure at the Oregon margin where the Pacific plate is subducting beneath the North American plate in general. The landward vergence structure may be an active structure that is supported by the occurrence of many landslide deposits and the topography. A bottom simulating reflector (BSR) is seen around the Kanasunose knoll (Fig. IV-6; shot #70-350). A BSR shows a base of a gas hydrate stability zone in sediments. The BSR depth varies from 0.2 to 0.4 seconds below the seafloor, that basically depends on the topography. The BSR depth is the shallowest at the top of the Kanasunose knoll. However, the BSR encounters the seafloor at shot #350. This may suggest that the sediments above the BSR were removed by slope failure, related to active landward vergent tectonics.

Enshu Fault Zone

MCS-26 runs from the No.2 Atsumi knoll (shot #400-900) to the Enshu fault zone (shot #1450-1950) (Fig. IV-11). The No.2 Atsumi knoll is bounded by reverse faults at its northern and southern limits. The Enshu fault zone are composed of three major faults, each showing a flower structure, pointing to a strike slip faulting. The topography of Enshu fault zone area shows step-like displacement; suggesting that the faults have a dip-slip components too. However, the strike-slip component may be dominant rather than dip slip from the topographical point of view. The most submarine canyons close to the faults are displaced to the dextrally, and the acoustic imagery of wade-range side-scan sonar data shows extremely strait lineaments (Kuramoto *et al.*, 1998). This interpretation is also supported by deep-towed multi-sensor data (see Kuramoto *et al.*, this volume). The northeastern fault of the Enshu fault zone could be an active fault and may continue more than 100 km. However the fault is divided into several segments based on an acoustic imagery (kuramoto *et al.*, 1998). The Enshu fault zone must be paid much attention to from an earthquake hazard point of view.

Deformation Front

MCS-29 and 31 cross almost the entire off Tokai accretionary wedge that is perpendicular to the general structural trend of the accretionary wedge. Especially, the deformation front is focused in this report (Fig. IV-12 to 15, from west to east). There are many variations of deformation style in the first deformation area. Some thrusts are imaged through the faults have small offsets. This suggests that the data have a high

resolution. However, the décollement reflector is not imaged clearly. An intense reflector at shot #1400-1520, 4.8-4.5 sec. depth (Fig. IV-15) may correspond to the "shallow detachment fault" that was pointed out by Chamot-Rook *et al.* (1992). It is impossible to recognize the reflector from a fault or displaced strata by the current MCS profiles. We must process the data much more.

Summary

The MCS data of GH97 and GA97 have a high resolution data quality. This report showed only preliminary processed data and pointed out some interesting features of this survey area. We will process the data by much more precise methods and much further interpret using the acoustic imagery map that of Kuramoto *et al.* (1998). We also aim at estimating the velocity structure from the MCS data. This may help the interpretations from physical property point of view. It is also very important point to evaluate an activity of active faults.

References

Chamot-Rooke, N., Lallemant, S.J., Le Pichon, X., Henry, P., Sibuet, M., Boulegue, B., Foucher, J.P., Furuta, T., Gamo, T., Glacon, G., Kobayashi, K., Kuramoto, S., Ogawa, Y., Schultheiss, P., Segawa, J., Takeuchi, A., Tarits, P. and Tokuyama, H. (1992) Tectonic context of fluid venting at the toe of the eastern Nankai accretionary prism: Evidence for a shallow detachment fault. *Earth Planet. Sci. Lett.*, **109**, 319-332.

Kuramoto, S., Kisimoto, K., Nakao, S., Tokuyama, H., Yamamoto, F. and Taira, A. (1998) *Seafloor acoustic imagery map of the off Tokai area.* Geological Survey of Japan Miscellaneous map series No. 37.

MacKay, M.E., Moore, G.F., Cochrane, G.R., Moore, J.C. and Kulm, L.D. (1992) Landward vergence and oblique structural trends in the Oregon margin accretionary prism: Implications and effect on fluid flow. *Earth Planet. Sci. Lett.*, **109**, 477-491.

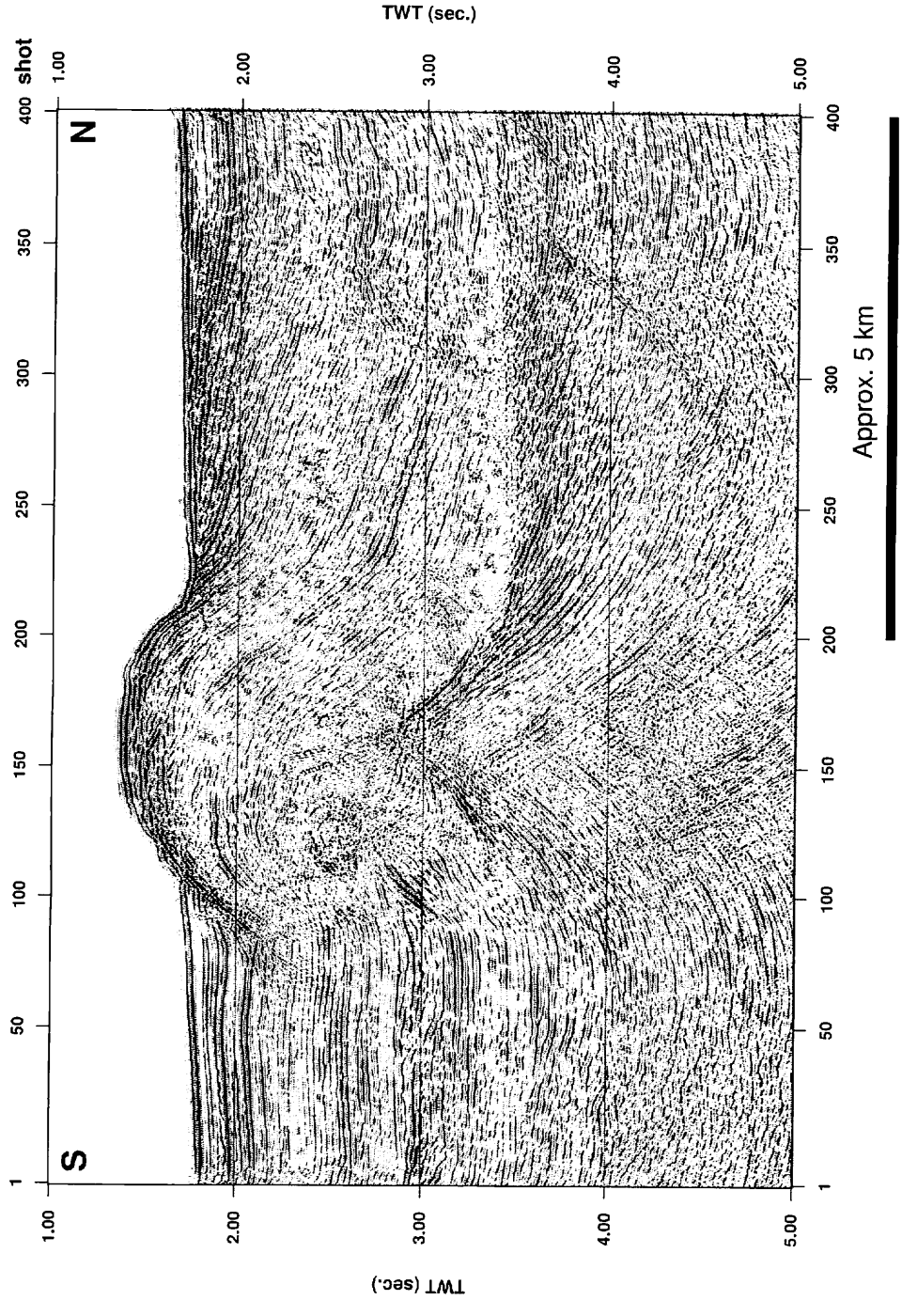

Fig. IV-3 Migrated profile of the MCS-04 line (time section).

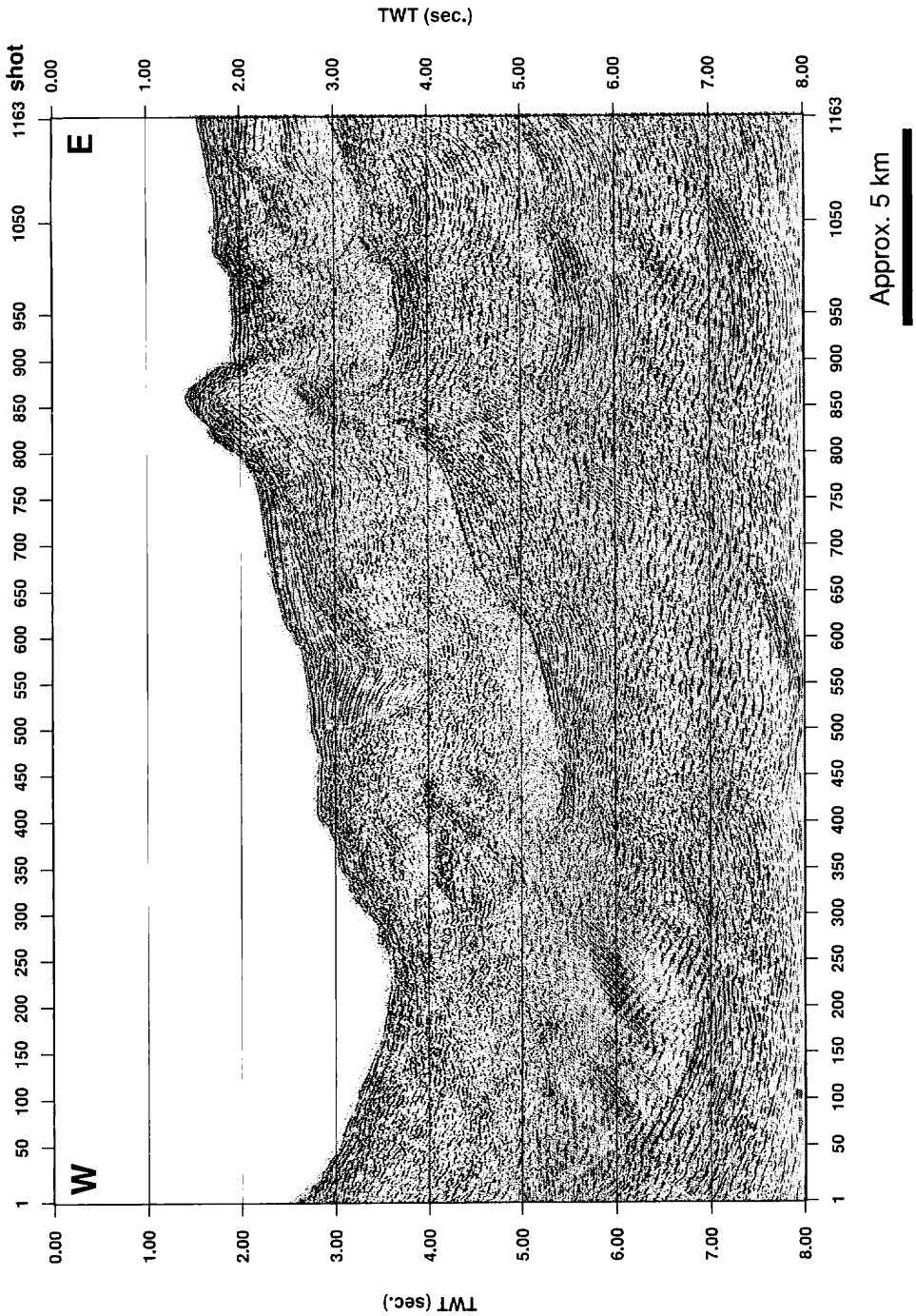

Fig. IV-4 Migrated profile of the MCS-10 line (time section).

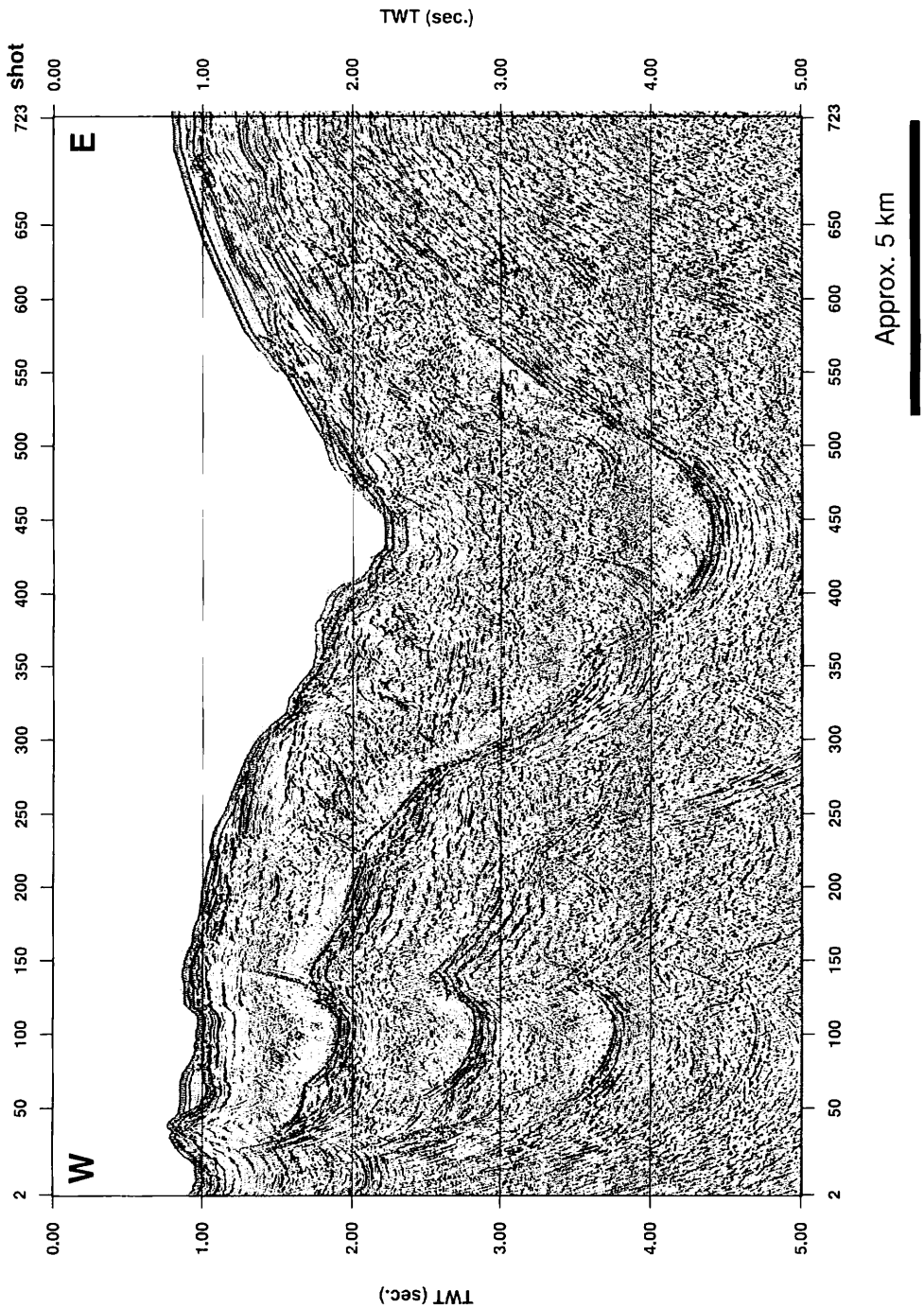

Fig. IV-5 Migrated profile of the MCS-18 line (time section).

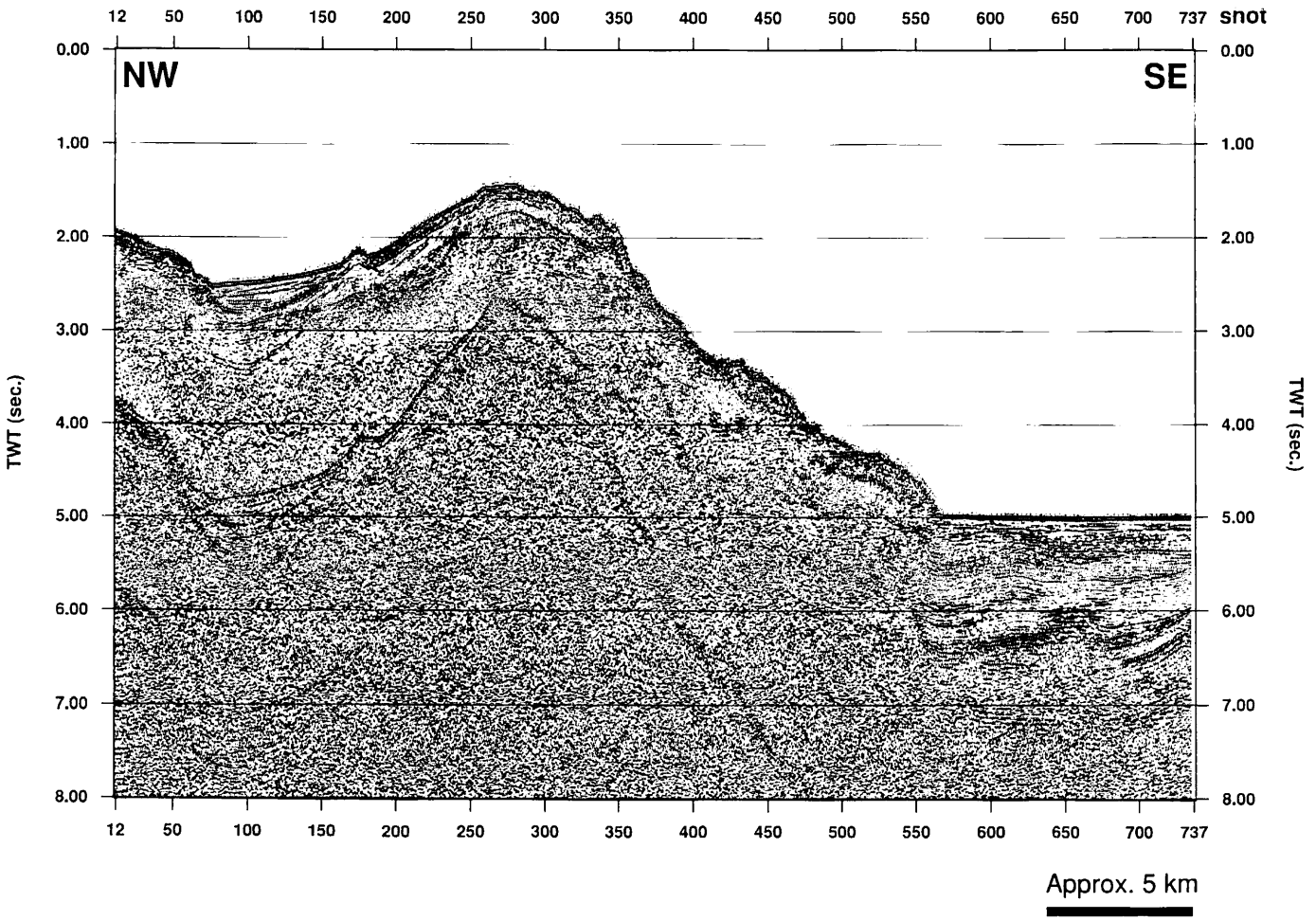

Fig. IV-6 Migrated profile of the GA-01 line (south; time section).

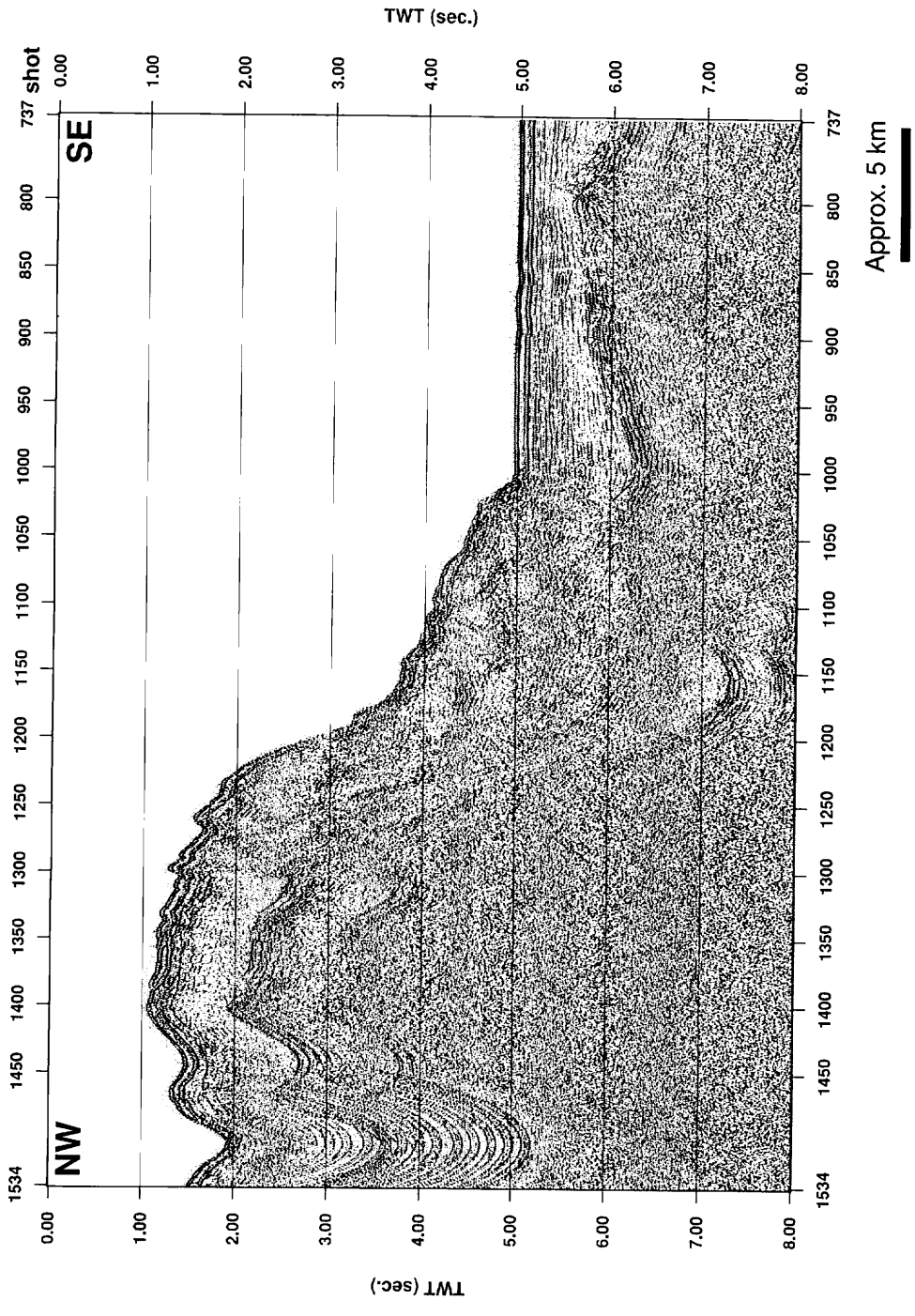

Fig. IV-7 Migrated profile of the GA-01 line (north; time section).

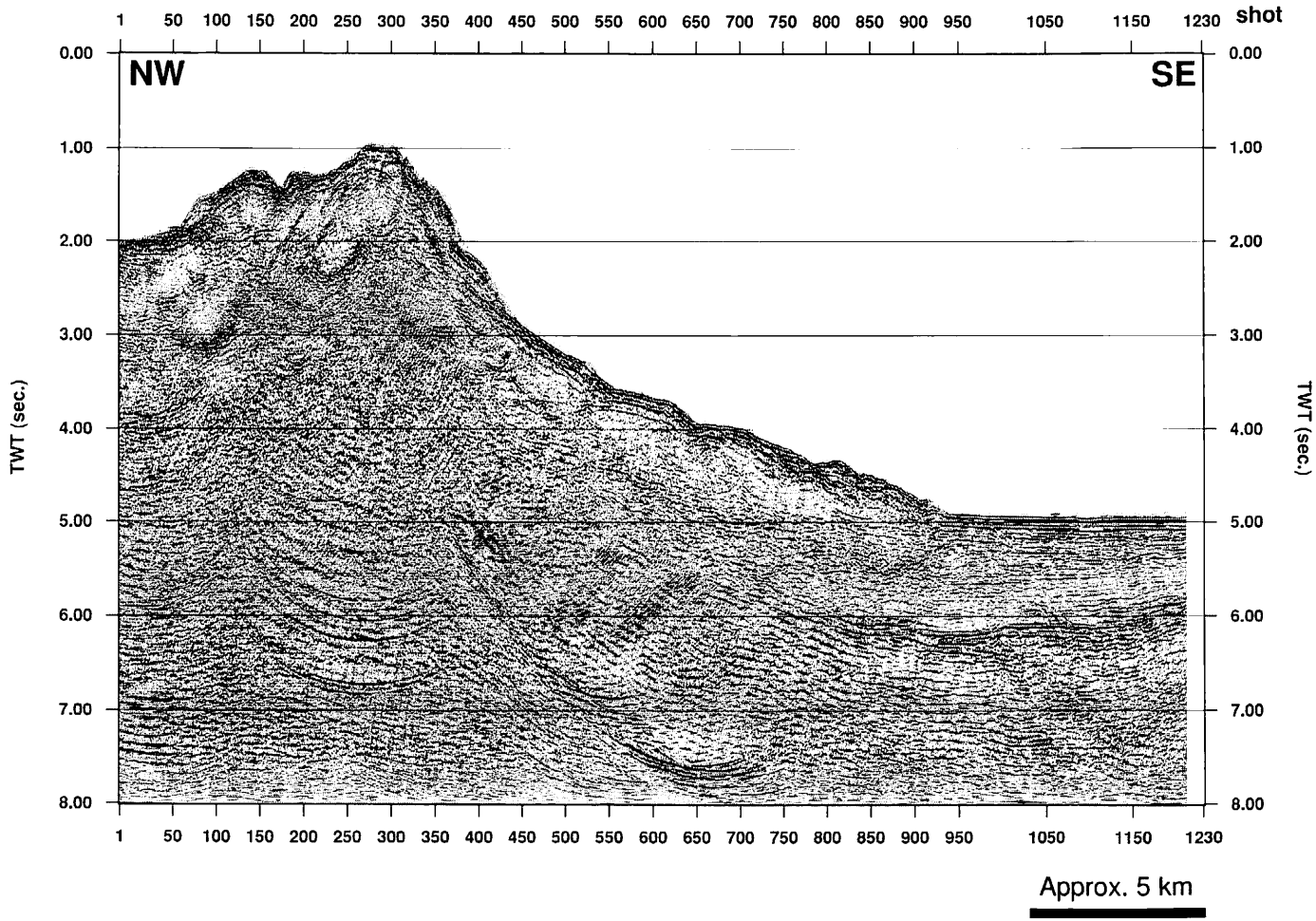

Fig. IV-8 Migrated profile of the MCS-20 line (west; time section).

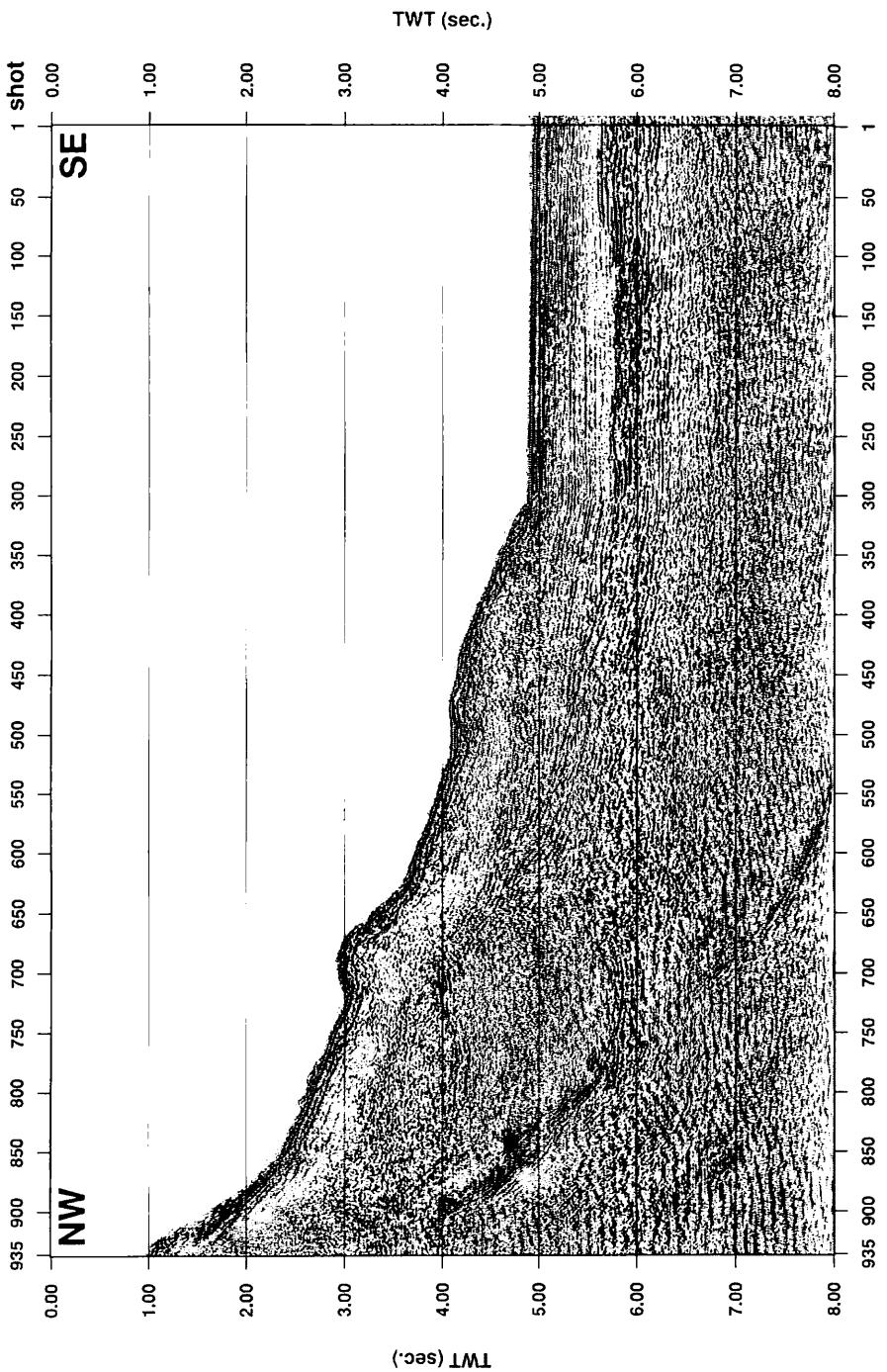

Fig. IV-9 Migrated profile of the MCS 20 line (middle; time section).

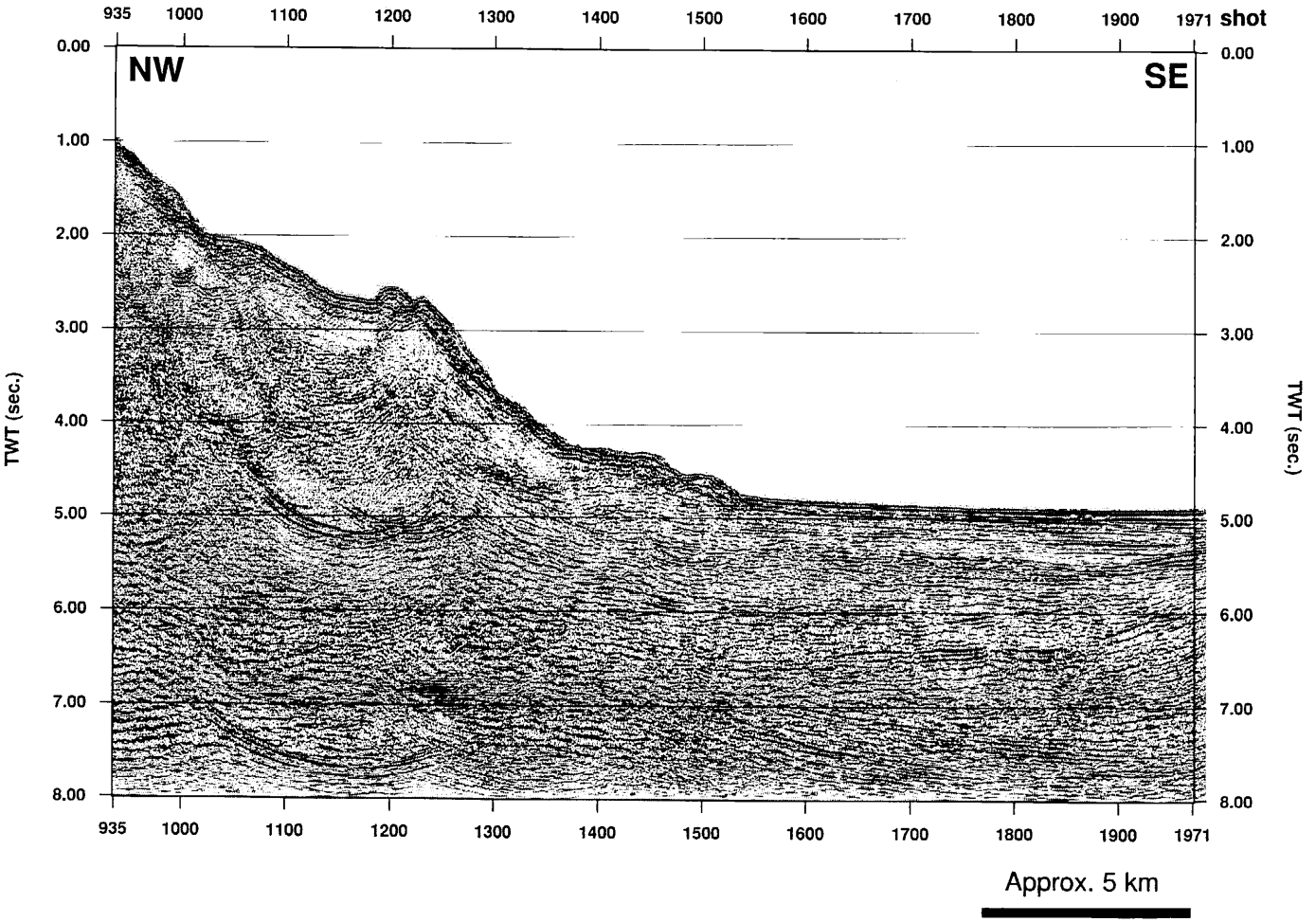

Fig. IV-10 Migrated profile of the MCS-20 line (east; time section).

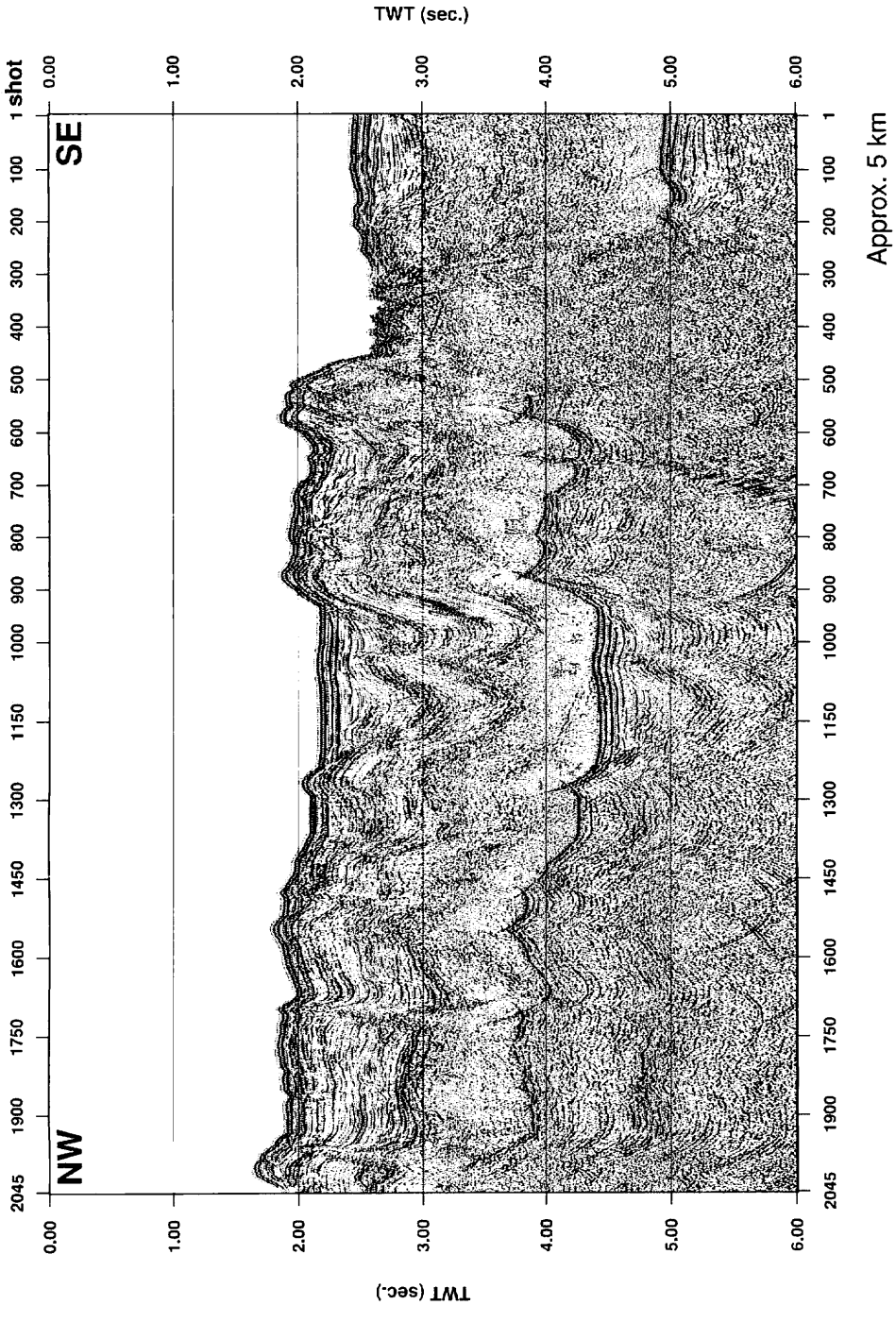

Fig. IV-11 Migrated profile of the MCS-26 line (time section).

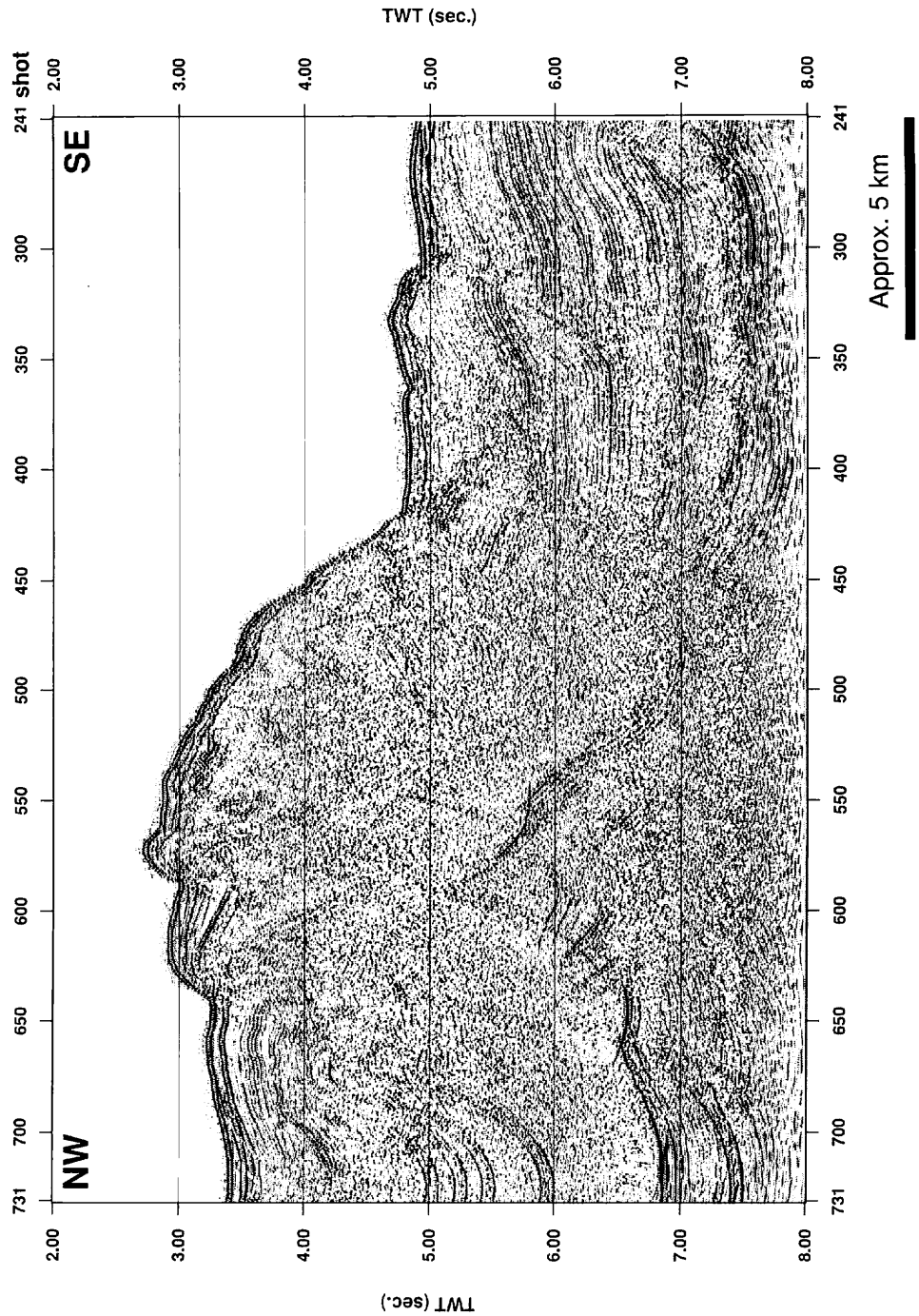

Fig. IV-12 Migrated profile of the MCS-29 line (west; time section).

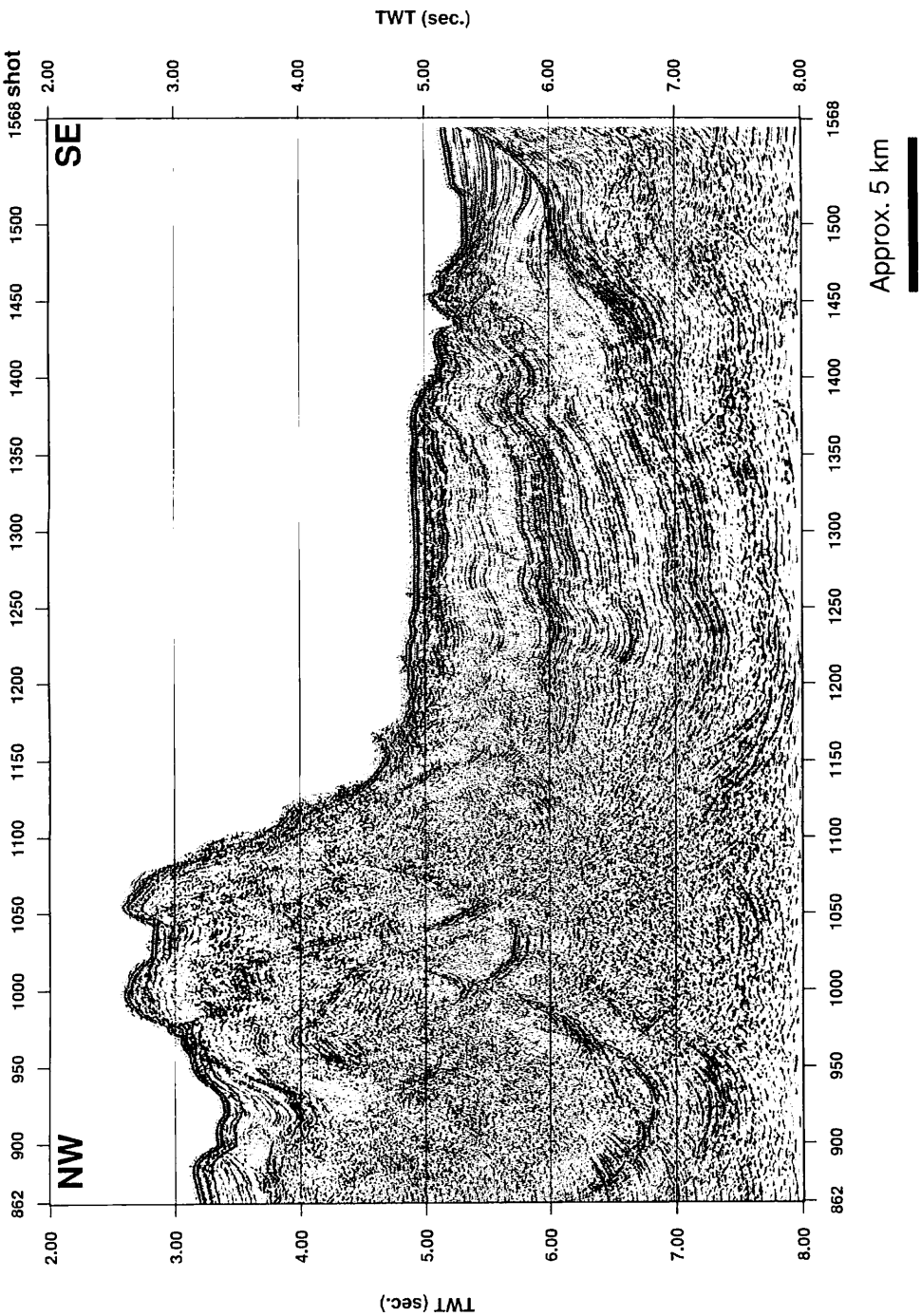

Fig. IV-13 Migrated profile of the MCS-29 line (east: time section).

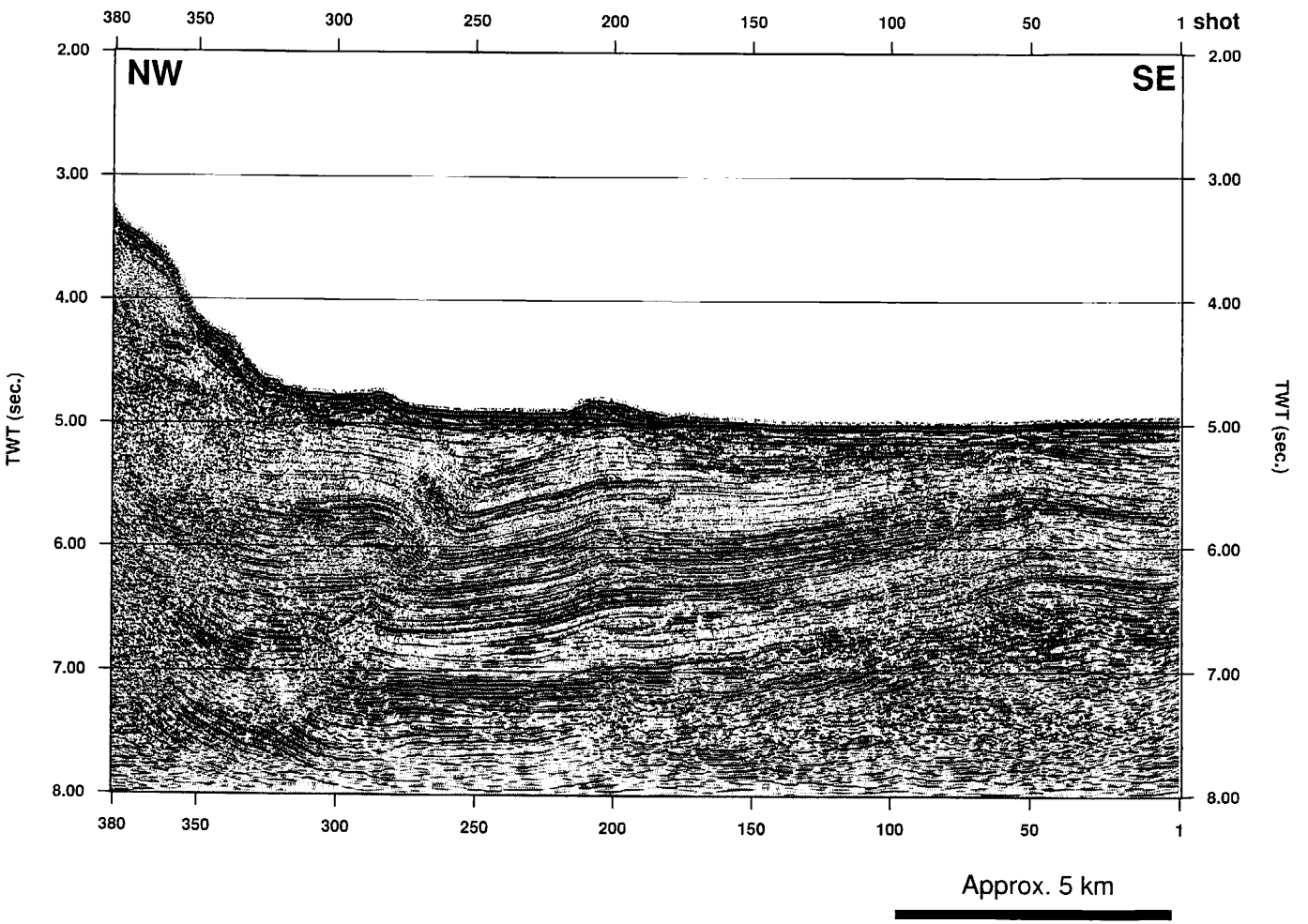

Fig. IV-14 Migrated profile of the MCS-31 line (west; time section).

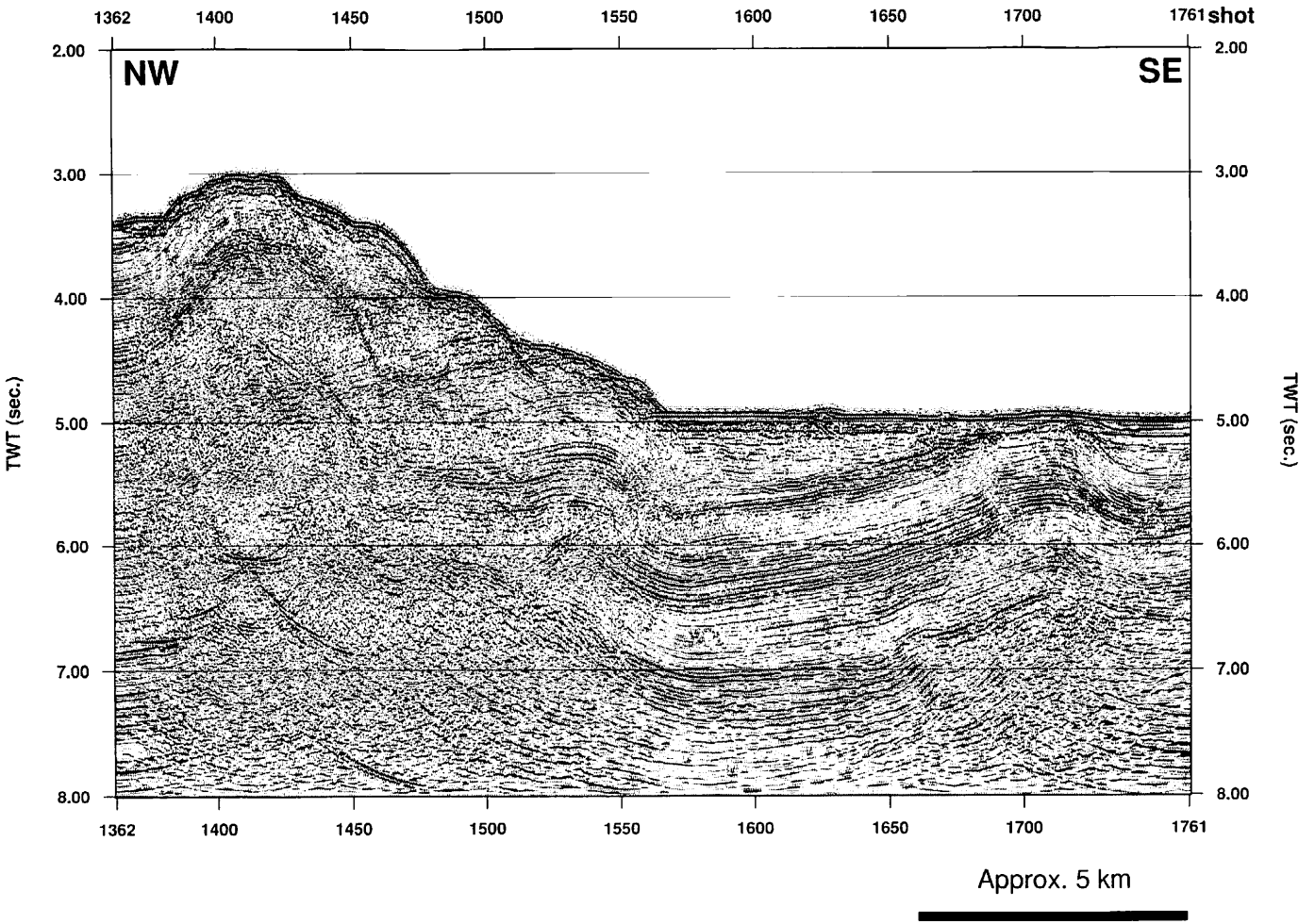

Fig. IV-15 Migrated profile of the MCS-31 line (east; time section).